COSTA, J., PEIXOTO, J., MOREIRA, P., SOUTO, A.P., FLORES, P., LANKARANI, H.M., INFLUENCE OF THE HIP JOINT MODELING APPROACHES ON THE KINEMATICS OF HUMAN GAIT. ASME JOURNAL OF TRIBOLOGY, VOL. 138(3), 031201, 10 PAGES, 2016.

Influence of the Hip Joint Modeling Approaches on the Kinematics of Human Gait

João Costa
Departamento de Engenharia Mecânica
Universidade do Minho, Campus de Azurém
4804-533 Guimarães, Portugal
E-mail: joaopmoraiscosta@gmail.com

Joaquim Peixoto
2C2T/Department of Textile Engineering
Universidade do Minho, Campus de Azurém
4804-533 Guimarães Portugal
E-mail: jjorge@det.uminho.pt

Pedro Moreira
Departamento de Engenharia Mecânica
Universidade do Minho, Campus de Azurém
4804-533 Guimarães, Portugal
E-mail: pfsmoreira@dem.uminho.pt

António Pedro Souto
2C2T/Department of Textile Engineering
Universidade do Minho, Campus de Azurém
4804-533 Guimarães Portugal
E-mail: souto@det.uminho.pt

Paulo Flores
Departamento de Engenharia Mecânica
Universidade do Minho, Campus de Azurém
4804-533 Guimarães, Portugal
E-mail: pflores@dem.uminho.pt

Hamid M. Lankarani
Department of Mechanical Engineering,
Wichita State University
Wichita, KS 67260-133
E-mail: hamid.lankarani@wichita.edu

ABSTRACT

The influence of the hip joint formulation on the kinematic response of the model of human gait is investigated throughout this work. To accomplish this goal, the fundamental issues of the modeling process of a planar hip joint under the framework of multibody systems are revisited. In particular, the formulations for the ideal, dry, and lubricated revolute joints are described and utilized for the interaction of femur head inside acetabulum or the hip bone. In this process, the main kinematic and dynamic aspects of hip joints are analyzed. In a simple manner, the forces that are generated during human gait, for both dry and lubricated hip joint models, are computed in terms of the system's state variables and subsequently introduced into the dynamics equations of motion of the multibody system as external generalized forces. Moreover, a human multibody model is considered, which incorporates the different approaches for the hip articulation, namely ideal joint, dry, and lubricated models. Finally, several computational simulations based on different approaches are performed, and the main results presented and compared to identify differences among the methodologies and procedures adopted in this work. The input conditions to the models correspond to the experimental data capture from an adult male during normal gait. In general, the obtained results in terms of positions do not differ significantly when the different hip joint models are considered. In sharp contrast, the velocity and acceleration plotted vary significantly. The effect of the hip joint modeling approach is clearly measurable and visible in terms of peaks and oscillations of the velocities and accelerations. In general, with the dry hip model, intra-joint force peaks can be observed, which can be associated with the multiple impacts between the femur head and the cup. In turn, when the lubricant is present, the system's response tends to be smoother due to the damping effects of the synovial fluid.

Keywords: Hip articulation, Ideal joint, Dry joint, Lubricated joint, Kinematics, Dynamics, Multibody model

1. INTRODUCTION

Over the last decade, various multibody models have been proposed for human gait analysis, which are typically capable of including the complex behavior associated with the soft tissues such as the muscles, tendons and ligaments [1-7]. In sharp contrast, the influence of the human articulation formulation on the predicted kinematics of the models of human gait has not been extensively investigated [8-12]. In fact, the majority of the studies on the modeling of natural and artificial human joints are not integrated in a whole multibody human model.

Piazza and Delp [13] are among the very few researchers who incorporated realistic human joint characteristics in a lower-limb multibody model. They proposed a rigid body approach of a total knee replacement performing a step-up task. Patterns of muscle activity and kinematics of the hip were measured experimentally and considered as inputs to the simulation. The model included the tibio-femoral and patello-femoral interactions, and predicted the flexion-extension pattern of the step-up activity. The contact problem between the knee joint elements was based on the linear complementarity problem [14]. More recently, Guess [15] presented a complete three-dimensional knee model developed within the framework of multibody systems. This study combined data from a cadaver-based natural knee model together with a muscle driven forward dynamics model from a human volunteer subject with similar height and weight. The knee model was utilized for the prediction of joint contact mechanics. This knee model also included the menisci. Quental et al. [16] proposed a robust and complete musculo-skeletal model of the upper limb to serve as the basis for the study of different types of shoulder pathologies, including the use of anatomical or reverse prostheses. The muscle system includes 21 muscles and the muscle contraction dynamics was represented by the Hill-type muscle model.

In general, much of the research work developed with the purpose of modeling and simulation of daily human tasks is based on the assumption that the human articulations, that constrain the system's components, are considered as ideal or perfect joints, such as spherical, revolute and universal joints. Dumas and his co-workers [17] performed a comparative study on the influence of using different kinematic joint models on the lower-limb musculo-tendon forces and joint reaction forces during human gait. The authors concluded that the musculo-skeletal model with a limited number of degrees-of-freedom and with some angle-dependent joint coupling and stiffness seems to provide satisfactory musculo-tendon forces and joint reaction forces. Nevertheless, with this approach, significant decrease in the kinematic precision compared with the living body could occur because the idealized models fail to capture the more complex aspects of joint kinematics [18]. However, the physical and mechanical properties of the natural and artificial human articulations including the effects of friction, lubrication and intra-contact force joints were neglected.

In the scientific field of mechanical systems' dynamics, several approaches for the representation of real physical mechanical joints, that is, joints' models that take into consideration their geometry, friction, wear and lubrication phenomena, have been developed [19-27]. However, these joint types have not been properly considered in the context of biomechanics of human gait. In order to increase the rigor of the articulation models of the human body, it is necessary to accurately describe the characteristics (geometric, physical and anatomical) of the human biological articulations, from the simple ones, such as the hip joint [28], to the most complex ones, such as the knee joint [29].

The present work deals with the dynamic modeling and analysis of human hip articulation for capturing some of its complexity while retaining the computational efficiency. This study, developed under the framework of multibody systems methodologies, extends the authors' previous work [30] to include the formulations for contact and lubrication actions into the hip joint multibody model. In a simple manner, the fundamental kinematic aspects of the hip joint are computed and used to evaluate the intra-hip joint forces for both dry and lubricated models. These joint forces are calculated based on the geometric, material, and mechanical properties of the components that constitute natural and artificial hip articulations. For both cases, the joint reaction forces are incorporated into the dynamic equations of motion as external generalized forces. The proposed approach is shown to be effective in obtaining a better understanding of the complex mechanical response of hip joint structures and its possible interactions with the human musculo-skeletal system.

The presentation of this study is organized as follows. Following the introduction, the fundamental kinematic aspects related to hip joint motion, such as the relative displacements and velocities are briefly revisited in Section 2. The kinematic parameters play a crucial role in the evaluation of the hip joint reaction forces during the dynamic analysis of the system. In Section 3, the constitutive laws for the dry and lubricated models are presented. For the dry contact case, the contact-impact forces are determined by employing a continuous force model based on the Hertzian contact theory. In turn, for the lubricated case, the forces developed due to the squeeze and wedge actions are evaluated from the hydrodynamic lubrication theory. The main ingredients of the multibody systems methodologies are summarized in a review manner in Section 4. A demonstrative example of application is presented in Section 5, which includes a planar human multibody model with the different approaches for the simulation of the hip joint. The results from the various simulations with different modeling approaches are provided in Section 6. Finally, the main conclusions of this study are drawn in the last section.

2. KINEMATICS OF THE HIP JOINT

In traditional analysis of planar multibody systems the human hip articulation can be modeled as an ideal or perfect joint, i.e., clearance, local elastic deformations, wear, and lubrication effects are neglected. However, in a real human joint, a gap is present between the femur head and hip bone or acetabulum. Such clearance is necessary to permit the relative motion between the connected bodies as well as to permit the components assemblage. This in essence is similar to a journal-bearing joint, while there is a radial clearance allowing for the relative motion between the journal and the bearing parts. For the ideal approach, the hip joint can be

considered as a ball and socket joint [31-34]. In this work the concept of journal-bearing model is considered with the purpose of keeping the analysis simple, but better representing the real physics of the hip joint because the human gait is confined to the sagittal plane [35].

From the modeling view point, the hip joint can be considered as a journal-bearing element, in which the gap between journal and bearing parts can be empty or filled with a lubricant (synovial fluid). With the purpose of determining the forces produced by a journal-bearing, the different kinematic parameters involved in the computation of these forces need to be identified. In standard multibody models, it is assumed that the connecting points of two bodies, linked by an ideal revolute joint, are coincident [36]. The introduction of the clearance in a revolute joint separates these two points and the bodies can freely move relative to each another. A revolute joint with clearance does not constrain any degree-of-freedom from the system like an ideal revolute joint. In a revolute clearance joint, the contact or lubrication forces control its dynamics. Thus, this type of joint can be identified as a force-interaction-joint, since it deals with force effects rather than the kinematic constraints.

Figure 1 shows a general configuration of a journal-bearing in a planar multibody mechanical system. The two bodies *i* and *j* are connected by a lubricated revolute joint, in which the gap between the bearing and the journal is filled with a fluid lubricant. Part of body *i* is the bearing and part of body *j* is the journal. The center of mass of body *i* is O_i and the center of mass of body *j* is denoted by O_j. Local coordinate systems for bodies *i* and *j* are attached to their centers of mass, while a global coordinate system is represented by *XY*. Point P_i indicates the center of the bearing and the center of the journal is referred by point P_j. The coordinate system *X'Y'* is parallel to the body fixed coordinate system $(\xi\eta)_i$ with its origin in the bearing center [37].

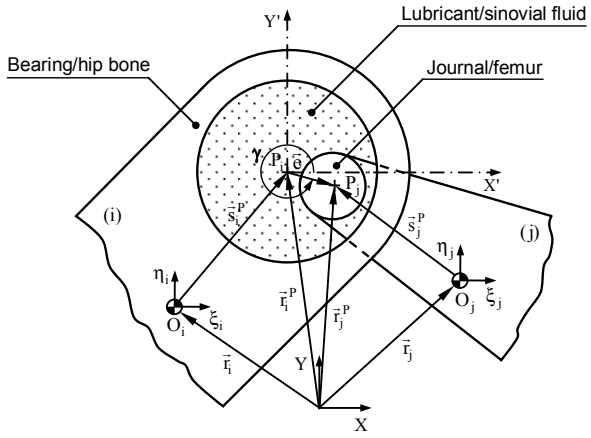

Figure 1: Journal-bearing in a planar multibody system representing the hip joint in this study

In what follows, some of the most relevant kinematic aspects associated with the journal-bearing are presented. As displayed in Fig. 1, the "eccentricity" vector **e**, which connects the centers of the bearing and journal, can be described as

$$\mathbf{e} = \mathbf{r}_j^P - \mathbf{r}_i^P \qquad (1)$$

where both $\mathbf{r}_j^P$ and $\mathbf{r}_i^P$ are position vectors written in global coordinates with respect to the inertial frame [36],

$$\mathbf{r}_k^P = \mathbf{r}_k + \mathbf{A}_k \mathbf{s}_k'^P, \quad (k=i,j) \qquad (2)$$

where $\mathbf{A}_k$ is the transformation matrix and $\mathbf{s}_k'^P$ is the vector of local coordinates of point *P* [36]. Equation (1) can be rewritten as

$$\mathbf{e} = \mathbf{r}_j^P + \mathbf{A}_j \mathbf{s}'^P_j - \mathbf{r}_i^P - \mathbf{A}_i \mathbf{s}'^P_i \qquad (3)$$

The magnitude of the eccentricity vector is evaluated as,

$$e = \sqrt{\mathbf{e}^T \mathbf{e}} \qquad (4)$$

where $\mathbf{e}^T$ is the transpose of vector **e**. A unit vector, **n**, along the eccentricity direction is defined can be defined as

$$\mathbf{n} = \frac{\mathbf{e}}{e} \qquad (5)$$

The unit radial vector **n** is aligned with the line of centers of the journal and bearing. The tangential direction is defined by rotating vector the radial vector **n** by an angle of 90º in the counter-clockwise direction.

For the case of dry revolute clearance joint, the contact between journal and bearing surfaces can be quantified by a pseudo-penetration, δ. In multibody system dynamics with contacting bodies, the words "penetration", "deformation", or "indentation" usually have the same meaning. In fact, the contact detection is performed by evaluating, at each integration time step, the gap or distance between potential contacting points. When this distance becomes negative, it means that the bodies overlap, and in these situations, the distance is designated as indentation or pseudo-penetration. In reality, the bodies do not penetrate each other, but they deform. In computational simulations, the pseudo-penetration is related to the actual local deformation of the bodies. Furthermore, in the second phase of the contact modeling problem, the application of the contact law deals with the use of an appropriate constitutive law relating the material properties and penetration to the contact forces necessary to avoid the indentation of the contacting bodies. In other words, the contact force can be thought of penalizing the indentation. Thus, it is clear that the geometric condition for contact between the bearing and journal can be defined as

$$\delta = e - c \tag{6}$$

where e is the magnitude of the eccentricity vector given by Eq. (4) and c is the radial clearance size. It should be noted that here the clearance is taken as a specified parameter based on clinical data. When the magnitude of the eccentricity vector is smaller than the radial clearance size, there is no contact between the journal and bearing surfaces. When the magnitude of eccentricity is larger than radial clearance, there is contact between the journal and the bearing, being the relative penetration given by Eq. (6). The contact or control points on bodies i and j are Q_i and Q_j, respectively. The global position of the contact points in the bearing and journal are given by [38]

$$\mathbf{r}_k^Q = \mathbf{r}_k + \mathbf{A}_k \mathbf{s}_k'^Q + R_k \mathbf{n}, \quad (k=i,j) \tag{7}$$

where R_i and R_j are the bearing and journal radius, respectively.

The velocities of the contact points Q_i and Q_j in the global system are obtained by differentiating Eq. (7) with respect to time, yielding

$$\dot{\mathbf{r}}_k^Q = \dot{\mathbf{r}}_k + \dot{\mathbf{A}}_k \mathbf{s}_k'^Q + R_k \dot{\mathbf{n}}, \quad (k=i,j) \tag{8}$$

Let the components of the relative velocity of contact points in the normal and tangential direction to the surface of collision represented by $\mathbf{v}_N$ and $\mathbf{v}_T$, respectively. The relative normal velocity determines whether the bodies in contact are approaching or separating, and the relative tangential velocity determines whether the bodies in contact are sliding or sticking [39]. The relative scalar velocities, normal and tangential to the surface of collision, v_N and v_T, are obtained by projecting the relative impact velocity onto the tangential and normal directions, yielding

$$\mathbf{v}_N = [(\dot{\mathbf{r}}_j^Q - \dot{\mathbf{r}}_i^Q)^T \mathbf{n}]\mathbf{n} \tag{9}$$

$$\mathbf{v}_T = (\dot{\mathbf{r}}_j^Q - \dot{\mathbf{r}}_i^Q)^T - \mathbf{v}_N \equiv v_T \mathbf{t} \tag{10}$$

where **t** is the tangential direction to the impacting surfaces.

The parameter ε, which defines the "eccentricity ratio", is the ratio between the distance from the bearing to the journal centers and the radial clearance, that is

$$\varepsilon = \frac{e}{c} \tag{11}$$

Parameter $\dot{\varepsilon}$ is obtained by differentiating Eq. (3) and dividing the result by radial clearance. Differentiating Eq. (3) yields

$$\dot{\mathbf{e}} = \dot{\mathbf{r}}_j^P + \dot{\mathbf{A}}_j \mathbf{s}'^P_j - \dot{\mathbf{r}}_i^P - \dot{\mathbf{A}}_i \mathbf{s}'^P_i \tag{12}$$

Hence, the time rate of eccentricity ratio is given by

$$\dot{\varepsilon} = \frac{\dot{e}}{c} \tag{13}$$

The line of centers between the bearing and journal makes an angle γ with X'-axis, as shown in Fig. 1. Since the unit radial vector **n** has the same direction as the line of centers, the angle γ is calculated using the following relation

$$\begin{Bmatrix} \cos\gamma \\ \sin\gamma \end{Bmatrix} = \begin{Bmatrix} n_x \\ n_y \end{Bmatrix} \tag{14}$$

from which,

$$\gamma = \tan^{-1}\frac{n_y}{n_x} \tag{15}$$

Thus, the parameter $\dot{\gamma}$ is obtained by differentiating Eq. (15) with respect to the time, yielding

$$\dot{\gamma} = \frac{e_x\dot{e}_y - \dot{e}_x e_y}{e^2} \tag{16}$$

In short, the contact problem studied within the framework of multibody systems formulations can be divided into two main phases, namely (*i*) the contact detection [40] and (*ii*) the application of an appropriate contact force law [41]. The contact detection is the procedure which allows to check whether the potential contacting surfaces are in contact or not. For multibody systems, this analysis is performed by evaluating, at each integration time step, the gap or distance between contacting points. When this distance becomes negative, it means that the bodies overlap, and hence in these situations, the distance is designated as penetration or indentation. In realty, the bodies do not penetrate each other, but they deform. In computational simulations, the penetration is related to the actual deformation of the bodies. In the second phase of the contact modeling problems, the application of the contact law deals with the use of an appropriate constitutive law relating the penetration and the contact forces necessary to avoid the inter-penetration of the contacting bodies. In other words, the contact force can be thought of penalizing the pseudo-penetration, and hence this approach is commonly denominated as penalty method.

In turn, when the space between the journal and bearing is filled with a lubricant, the joint becomes a revolute joint with lubrication action, whose kinematic are aspects similar to those for the revolute joint with clearance. The only difference is that the relative radial velocity expressed by Eq. (8) leads the lubricant squeeze action when there is no contact between the journal and bearing walls.

3. DYNAMICS OF THE HIP JOINT

For the case of dry clearance approach, the contact-impact forces can be obtained by using one of the Hunt-Crossley models [42-44]. This approach is sound since that models account for both the elastic and damping effects, in particular those that involve spherical contacting surfaces. The damping effect is associated with the energy dissipated during the impact process, together with the dissipative effect associated with the Coulomb friction on the contact surfaces [45].

Various types of constitutive laws are suggested in the literature [46-50], all based one of original prominent model proposed by Hertz. However, the Hertz contact model law is purely elastic in nature and cannot explain the energy loss during the impact process. Lankarani and Nikravesh [43] overcame this difficulty by separating the normal contact force into elastic and dissipative components as

$$f_N = K\delta^n + D\dot{\delta} \tag{17}$$

where the first term represents the elastic forces and the second term accounts for the energy dissipation. In Eq. (17), K is the generalized contact stiffness parameter, δ is the relative penetration depth, D is the hysteresis damping coefficient and $\dot{\delta}$ is the relative impact velocity. The exponent n is set equal to 1.5 for most metallic contacts. The generalized stiffness parameter K depends on the geometry and physical properties of the contacting surfaces. For two spherical contacting bodies with radii R_i and R_j, the stiffness parameter is expressed by [51]

$$K = \frac{4}{3(\sigma_i + \sigma_j)}\left[\frac{R_i R_j}{R_i + R_j}\right]^{\frac{1}{2}} \tag{18}$$

where the material parameters σ_i and σ_j are given by

$$\sigma_z = \frac{1-\nu_z^2}{E_z}, \quad (k=i,j) \tag{19}$$

in which the variables ν_z and E_z denote the Poisson's coefficient and Young's modulus associated with each body, respectively.

The hysteresis damping coefficient D can be expressed by [43]

$$D = \eta\delta^n \tag{20}$$

where η is the hysteretic damping factor. An expression for η can be obtained by relating the kinetic energy loss by the impacting bodies to the energy dissipated in the system due to internal damping. Considering the kinetic energies before and after impact, the energy loss ΔE can be expressed as a function of the restitution coefficient c_e and initial impact velocity $\dot{\delta}^{(-)}$

$$\Delta E = \tfrac{1}{2} m\dot{\delta}^{(-)^2}(1-c_e^2) \tag{21}$$

where c_e is the "coefficient of restitution".

The energy loss can also be evaluated by the integration of the contact force around the hysteresis loop. Assuming that the damping force deformation characteristics during the loading and unloading phases are the same, it can be seen that [43]

$$\Delta E = \oint D\dot{\delta}\,d\delta \approx 2\int_0^{\delta_{\max}} \eta\delta^n\dot{\delta}\,d\delta \approx \frac{2}{3}\frac{\eta}{K} m\dot{\delta}^{(-)^3} \tag{22}$$

After substituting Eq. (21) in Eq. (22) an expression for the hysteretic damping factor η is obtained as

$$\eta = \frac{3K(1-c_e^2)}{4\dot{\delta}^{(-)}} \tag{23}$$

which represents the kinetic energy loss of the work done by the contact force. Thus, the hysteretic damping factor expressed by Eq. (23) is now substituted into Eq. (17) resulting in the continuous contact force model, which includes internal damping, written here as [43]

$$f_N = K\delta^n\left[1+\frac{3(1-c_e^2)}{4}\frac{\dot{\delta}}{\dot{\delta}^{(-)}}\right] \tag{24}$$

For the case of lubricated hip joints, the Reynolds' equation is utilized to evaluate the hydrodynamic forces developed by the fluid pressure field in a hip joint. When the journal and bearing have relative rotational velocities with respect to each other, the amount of eccentricity adjusts itself until the pressure generated in the converging lubricating film balances the external loads. The pressure generated, and hence the load capacity of the journal-bearing, depends on the journal eccentricity, the relative angular velocity, the effective viscosity of the fluid lubricant, and the journal-bearing geometry and clearance. There are two different actions of pressure generation in journal-bearings, namely the "wedge" and "squeeze" actions. The squeeze action relates the radial journal motion with the generation of load capacity pressure in the lubricant film, whilst the wedge action deals with the relation between relative rotational velocity of the journal and bearing ability to produce such pressure. When the journal and bearing walls are fully separated, the assumption of hydrodynamic lubrication theory can be applied [37]. This means that the hydrodynamic forces, which are developed due to the pressure field generated during their relative motion, control the dynamics of the journal and bearing elements. However, when the journal and bearings surfaces are too close, alternative lubrication theories must be considered, such as those presented in [9, 10].

The isothermal Reynolds' equation for a dynamically loaded journal-bearing for which the fluid is incompressible and the journal and bearing do not experience any elastic deformation, can be written as [52]

$$\frac{\partial}{\partial X}\left(\frac{h^3}{\mu}\frac{\partial p}{\partial X}\right)+\frac{\partial}{\partial Z}\left(\frac{h^3}{\mu}\frac{\partial p}{\partial Z}\right)=6U\frac{\partial h}{\partial X}+12\frac{dh}{dt} \tag{25}$$

where h is the fluid film thickness, p is the fluid pressure, μ is the absolute fluid viscosity, U is the relative tangential velocity, and X and Z are the radial and axial directions, respectively. The two terms on the right-hand side of Eq. (25) represent the two different effects of pressure generation on the lubricant film, i.e., wedge and squeeze film actions, respectively.

It is known that the Reynolds' equation (25) is a nonhomogeneous partial differential of elliptical type being the exact solution difficult to obtain and, in general, requiring considerable numerical effort. However, it is possible to solve the Reynolds' equation

analytically when either the first or the second term on the left-hand side is null. These particular solutions correspond to models of infinitely-short and infinitely-long journal-bearing, respectively.

For an infinitely-long journal-bearing it is assumed a constant fluid pressure and a negligible leakage in the *Z*-direction (referred to Fig. 1). In many cases, it is possible to treat a journal-bearing as infinitely-long and consider only its middle point. This solution, firstly presented by Sommerfeld [52], is valid for length-to-diameter ratios L_B/D_B greater than 2. Considering the case of an infinitely long journal-bearing, the Reynolds' equation is simplified as

$$\frac{\partial}{\partial X}\left(\frac{h^3}{\mu}\frac{\partial p}{\partial X}\right)=6U\frac{\partial h}{\partial X}+12\frac{dh}{dt} \tag{26}$$

By integrating Eq. (26), the pressure field in the journal-bearing is given by

$$p=6\mu\left(\frac{R_J}{c}\right)^2\left\{\frac{(\omega-2\dot{\gamma})(2+\varepsilon cos\theta)\varepsilon sin\theta}{(2+\varepsilon^2)(1+\varepsilon cos\theta)^2}+\frac{\dot{\varepsilon}}{\varepsilon}\left[\frac{1}{(1+\varepsilon\cos\theta)^2}-\frac{1}{(1+\varepsilon)^2}\right]\right\} \tag{27}$$

where again c is the radial clearance, θ is the angular coordinate, ε is the eccentricity ratio, $\dot{\varepsilon}$ is the time rate of change of eccentricity ratio, μ is the dynamic lubricant viscosity and R_J is the journal radius.

Equation (27) enables the calculation of the pressure distribution in a hydrodynamic infinitely-long journal-bearing as a function of the dynamic journal-bearing parameters and geometry. However, it is convenient to determine the force components of the resultant pressure field in the directions aligned and perpendicular to the line of centers of the journal and bearing. These force components can be obtained by integration of the pressure field around the half domain π, i.e., the pressure distribution is integrated only over the positive region by setting the pressure in the remaining portion equal to zero. These are known as the Gümbel's boundary conditions. This analysis involves a great deal of mathematical manipulation for which the interested reader is referred to [52]. Thus, the component forces along eccentricity direction and its perpendicular direction are, for $\dot{\varepsilon}>0$, given by

$$f_r=-\frac{\mu L_B R_J^3}{c^2}\frac{6\dot{\varepsilon}}{(2+\varepsilon^2)(1-\varepsilon^2)^{3/2}}\left[4k\varepsilon^2+(2+\varepsilon^2)\pi\frac{k+3}{k+3/2}\right] \tag{28}$$

$$f_t=\frac{\mu L_B R_J^3}{c^2}\frac{6\pi\varepsilon(\omega-2\dot{\gamma})}{(2+\varepsilon^2)(1-\varepsilon^2)^{1/2}}\frac{k+3}{k+3/2} \tag{29}$$

and for $\dot{\varepsilon}<0$ yields

$$f_r=-\frac{\mu L_B R_J^3}{c^2}\frac{6\dot{\varepsilon}}{(2+\varepsilon^2)(1-\varepsilon^2)^{3/2}}\left[4k\varepsilon^2-(2+\varepsilon^2)\pi\frac{k}{k+3/2}\right] \tag{30}$$

$$f_t=\frac{\mu L_B R_J^3}{c^2}\frac{6\pi\varepsilon(\omega-2\dot{\gamma})}{(2+\varepsilon^2)(1-\varepsilon^2)^{1/2}}\frac{k}{k+3/2} \tag{31}$$

where the parameter k is defined as

$$k^2=(1-\varepsilon^2)\left[\left(\frac{\omega-2\dot{\gamma}}{2\dot{\varepsilon}}\right)^2+\frac{1}{\varepsilon^2}\right] \tag{32}$$

in which L_B is the journal-bearing length, c is the radial clearance, ω is the relative angular velocity between the journal and the bearing and γ is the angle between the eccentricity direction and the *X*-axis, as depicted by Fig. 1. The notation $(\dot{\bullet})$ denotes the time derivative of the quantity $(\bullet)$. The hydrodynamic force components given by Eqs. (28) to (32) are nonlinear functions of the time parameters, ω, ε, $\dot{\varepsilon}$, γ, and $\dot{\gamma}$, which can be evaluated at any instant of time from the dynamic analysis of the multibody system. The journal's center motion is obtained from the dynamic analysis of the overall system.

4. MULTIBODY SYSTEMS FORMULATION

The dynamics equations of motion for a multibody system subjected to holonomic constraints can be described as [36]

$$\begin{bmatrix} \mathbf{M} & \mathbf{\Phi}_{\mathbf{q}}^{T} \\ \mathbf{\Phi}_{\mathbf{q}} & \mathbf{0} \end{bmatrix} \begin{Bmatrix} \ddot{\mathbf{q}} \\ \boldsymbol{\lambda} \end{Bmatrix} = \begin{Bmatrix} \mathbf{g} \\ \boldsymbol{\gamma} \end{Bmatrix} \tag{33}$$

with the reference frame placed at the center of mass for each body, $\mathbf{M}$ is the system mass matrix, $\mathbf{\Phi}_{\mathbf{q}}$ is the Jacobian matrix of constraint equations, the vector $\ddot{\mathbf{q}}$ contains the generalized state accelerations, $\boldsymbol{\lambda}$ is the vector that contains the Lagrange multipliers associated with systems ideal kinematic jonts, $\mathbf{g}$ is the vector of generalized forces and $\boldsymbol{\gamma}$ is the vector of quadratic velocity terms that is used to describe Coriolis and centrifugal terms in the equations of motion [36]. Equation (33) is formed as a combination of the equations of motion and kinematic acceleration equations, often referred to as a "mixed set of differential and algebraic equations".

A set of initial conditions (positions and velocities) is required to start the dynamic simulation. The selection of the appropriate initial conditions plays a key role in the prediction of the dynamic performance of mechanical system [53]. In the present work, the initial conditions are based on the results of kinematic simulation of a mechanical system in which all the joints are assumed to be ideal, that is, without clearance. The subsequent initial conditions for each time step in the simulation are obtained in the usual manner from the final conditions of the previous time step [36]. In order to stabilize or keep under control the constraints violation, Eq. (33) is solved using the Baumgarte stabilization technique [54, 55]. This method is utilized in this study due to its robustness, easiness to implement and mainly due to its computational efficiency. Alternative formulations are available in the literature, and the interested reader referred to the works by Nikravesh [36, 53].

In turn, the integration process is performed using a predictor-corrector algorithm with both variable step size and order [56, 57]. The use of numerical algorithms with automated adjustable time step size is particularly important in contact problems whose dynamic response is quite complex due to the sudden changes in kinematic configuration. In such events, the use of a constant time step is computationally inefficient and the system could be overlooked due to insufficient time resolution. The automated time step size adaptability is therefore a crucial part of the dynamic solution procedure. Additionally, the abrupt configuration changes caused by rapid variation of contact forces are source of normal stiffness, since the natural frequencies of the system are widely spread. Thus, the time step size must be adjusted in order to capture the fast and low components of the system response [36].

5. MODEL DEVELOPMET

This section includes the details of development of a human multibody models with different approaches for modeling of the hip joint. The human multibody model of the human body is developed and analyzed within a general purpose multibody code that uses a methodology based on multibody systems formulations [36]. Figure 2 shows a schematic representation of the human multibody model considered here. The model is composed of seven rigid bodies, including two legs (thigh, shank, foot) and the main body segments here denominated as HAT (acronym for Head-Arms-Trunk) [30]. The present study only accounts for the skeletal structure, and the effect of muscles, tendons and ligaments have been neglected [1].

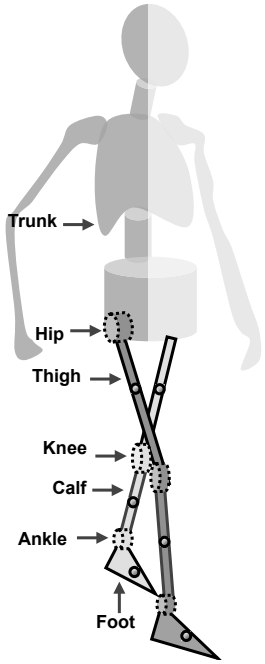

Figure 2: Two-dimensional human multibody model

It is well known that in order to define the configuration of a planar body, three independent coordinates are needed, namely, two coordinates specifying the translation of the body center of mass and one specifying the body rotation [36]. Since the model used here is two-dimensional (the human multibody model is considered for gait analysis in the "mid-sagittal plane"), it has a total of 21 Cartesian coordinates, which results from three coordinates for each body. An anthropometric description of the seven anatomical segments and their corresponding properties are listed in Table 1, which have been adopted from [58].

In the human multibody model considered in this study, six revolute joints link the anatomical segments, which result in twelve constraints in the system. Thus, the inclusion of these constraints to the system results in nine degrees-of-freedom, corresponding to six rotations for the revolute joints axes, plus two translations and one rotation of the main body (½ HAT). These nine degrees-of-freedom are associated with the "guiding constraints", as described in reference [30]. In addition to development of the guiding constraints, it is also necessary to have the kinetic information describing the interaction between the model and its surrounding environmental, namely the normal of contact forces on the feet, as well as their respective points of application [1]. The trajectories of all the bodies that represent the system's degrees-of-freedom have guide constraints associated, which are obtained experimentally. The motion data for the biomechanical system consists of the trajectory of a set of anatomical points located at the natural joints. The collected data points are then interpolated using cubic splines in order to define the necessary mathematical expressions that represent that guide constraint equations. The methodology utilized to model the guiding constraints associated with bodies' trajectories has been validated and incorporated in a specific computational code developed with the purpose of performing kinematic and dynamic analysis of human multibody models [59].

Table 1: Anthropometric data for each anatomical segment of the human multibody model

Segment	Description	Length [m]	Mass [kg]	Moment of inertia [kgm^2]
1	½ HAT	0.2575	19.221	1.03923
2	Right thigh	0.3141	5.670	0.05836
3	Right shank	0.4081	2.637	0.04005
4	Right foot	0.1221	0.822	0.00273
5	Left thigh	0.3141	5.670	0.05836
6	Left shank	0.4081	2.637	0.04005
7	Left foot	0.1221	0.822	0.00273

The values of the contact forces between the ground and feet are obtained from experiment [59]. Furthermore, it is clear that the point of application of these contact forces varies with time during the interaction between the foot and the ground along stance period. This issue is of paramount importance in order to obtain proper results, as it was demonstrated in [60-62]. Thus, in order to correctly define the point of application of reaction forces in the system, it is necessary to calculate the local coordinates of this point in relation to the center-of-mass of the foot [30].

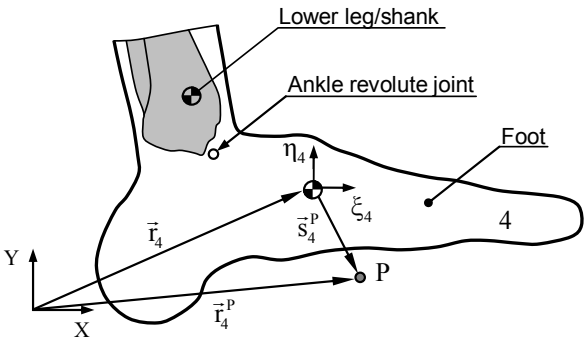

Figure 3: The shank-foot subpart of the human multibody model

Figure 3 shows the location of a generic point of application *P* of the contact forces developed between the foot and ground. The global coordinates of the contact point are given by [36]

$$\mathbf{r}_4^P = \mathbf{r}_4 + \mathbf{A}_4 \mathbf{s}_4^{'P} \qquad (34)$$

In addition, the Cartesian components of the applied external forces, here designated by f_x and f_y, have been transferred to the foot's center of mass. The transferred forces and moments are then added to the generalized force vector of the foot, resulting in the force components and a moment of forces. The reader interested in the detailed analysis of the human multibody modeling for locomotion is referred to the work by Silva and Ambrósio [1] and Meireles et al. [30].

As mentioned above, the human multibody model developed here is investigated for three different types of hip joint models, the ideal or perfect case, the dry clearance joint, and the lubricated joint. The traditional formulation for an ideal revolute joint, known as zero clearance approach, considers that the connecting points of two bodies linked by a revolute joint are coincident. The introduction of the clearance in a joint separates these two points. Thus, a revolute joint with clearance does not constraint any degree-of-freedom from the mechanical system like the ideal joint, it imposes some restrictions, limiting the journal to move within the bearing. In fact, when clearance is present in a revolute joint, the two kinematic constraints are removed and two degrees-of-freedom are introduced instead. The dynamics of the joint is then controlled by forces related to the interaction between the femur head and cup. Thus, whilst a perfect revolute joint in a mechanical system imposes kinematic constraints, a revolute clearance joint leads to force constraints. In short, when the hip articulation is modeled as an ideal joint, the corresponding kinematic constraints are introduced into the equations of motion in terms of Jacobian matrix ($\mathbf{\Phi_q}$) and right hand-side of the accelerations vector ($\boldsymbol{\gamma}$). In turn, for the cases of dry and lubricated models, the contribution to the equations of motion are reflected in terms of external forces that develop during the system's motion and are introduced into the generalized force vector ($\mathbf{g}$) [36].

6. RESULTS AND DISCUSSION

In this section, some results obtained from computational simulations of a human multibody model described in the previous section are presented and discussed. For this purpose, different approaches for modeling of the hip joint have been utilized. In order to keep the analysis simple and to improve the computational efficiency of the code, only one leg is considered in the simulations. This is clear due to the similarity and equivalence of the motion described in both legs, since the input data capture correspond to a male without any pathology in terms of human locomotion [58]. Table 2 presents the main parameters used in the different models, and to characterize the problem and for the numerical methods utilized. The main anthropometric, kinematic and kinetic information of the human multibody model described earlier is extracted from Ref. [30]. This data corresponds to a period of time equal to 0.957 s, representing a complete gait cycle of normal cadence [58]. The gait cycle is divided into two main phases. The first phase [0.0-0.4s] corresponds to the "swing period", while the second phase [0.4-0.957s] corresponds to the "stance period" [59]. The radial clearance of the nonideal hip joint is taken to be equal to 20 μm, which corresponds to the actual size in a typical hip prosthesis with nominal dimensions utilized in the present study [63]. It must be stated that in the present investigation, all computational simulations of human multibody model with different hip joint formulation under the same set of input conditions. The scenario and conditions have been considered when modeling the hip articulation with the three different approaches, which corresponds to the normal human gait, since the main purpose of this work is to deal with the hip joint model. Anyway, different scenarios could also be considered, namely those associated with the running, stair climbing, squatting, just to mention a few.

Table 2: Parameters used in the dynamic simulations of the human multibody model with nonideal hip joint

Hip nominal radius	32 mm	Friction coefficient	0.01
Radial clearance	20 μm	Fluid viscosity	500 Pas

Young's modulus	350 GPa	Baumgarte α, β	5
Poisson's ratio	0.3	Integration time step	1×10^{-6} s
Restitution coefficient	0.9	Integrator algorithm	Gear

The dynamic response of the human multibody model is quantified by plotting the position, velocity and acceleration of the thigh for the different models of the hip articulation. In addition, Poincaré maps are utilized to study the dynamic behavior of the human multibody model in terms of periodic and nonperiodic responses. For this purpose, the velocity and acceleration of the thigh in the vertical *Y*-direction are the kinematic variables to construct the Poincaré maps. It must be highlighted that in order to keep the analysis simple, the diagrams plotted here are only for the thigh and in the *Y*-direction. Nevertheless, similar results can be obtained for other variables and for other anatomical segments and directions.

Figures 4 up to 15 show the global results obtained from the computational simulations for the different hip joint models, for two different hip nominal radii and for two values of synovial fluid viscosity. As it would be excepted, the outcomes in terms of positions response are not significantly affected by the hip joint model considered. This is logical because the magnitude of the clearance is quite small when compared with the general dimensions of the anatomical segments and also with the gross motion described by the systems' elements.

However, the influence of the hip joint model in terms of the plots for velocities and accelerations is quite visible. Indeed, the variations and peaks observed are clearly associated with the intra-joint forces developed during the motion produced for dry and lubricated modeling approaches. The results indicate that the fluid lubricant acts like a damper, in the measure that it reduces the accelerations peaks visible for the dry joint. This is quite visible, mainly in the diagrams of accelerations. The effect of the fluid viscosity is also noticeable in the plots. In fact, when the viscosity is very high, such as for the case of 500 Pas, the systems tends to rigidify and the response is not very smooth. When the hip joint is modeled as lubricated with a viscosity of 250 Pas, it can be observed that system's response is much more smooth. It can be concluded that the dry joint model tends to exhibit a nonperiodic response due to the level of impacts between journal and bearing surfaces. The system's response is relatively close to the ideal joint case, when the hip joint is modeled as a lubricated one, as Poincaré maps indicate.

Finally, it must be stated that the simulation results for the ideal, dry, and lubricated joint models present a close response in terms of the variables plotted. This is logical since the values of the clearance considered are quite small when compared with the global motion produced. However, a significant deviation can be observed when highly values for the clearance are used. Moreover, when the fluid has a very low viscosity, the system's response exhibit a more complex pattern in the measure that the journal and bearing walls move quite close to each other.

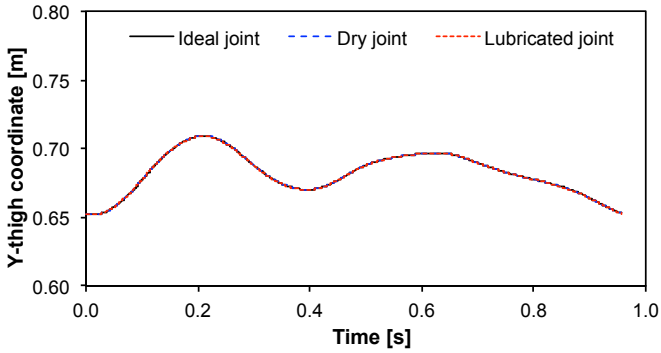

Figure 4: Y-position of the thigh for a complete gait cycle (hip radius of 32 mm, radial clearance of 20 µm; viscosity of 500 Pas)

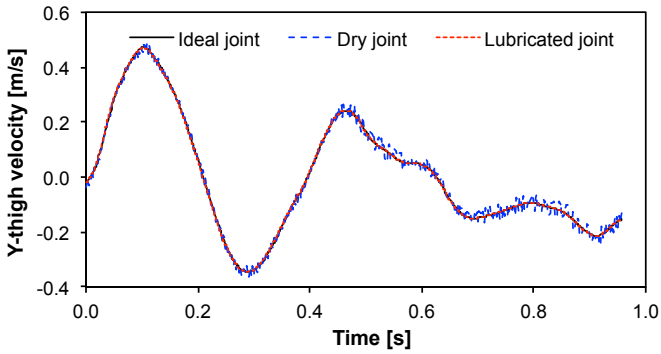

Figure 5: Y-velocity of the thigh for a complete gait cycle (hip radius of 32 mm, radial clearance of 20 µm; viscosity of 500 Pas)

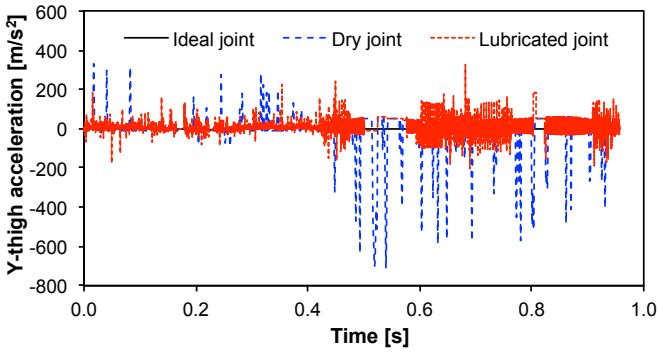

Figure 6: Y-acceleration of the thigh for a complete gait cycle (hip radius of 32 mm, radial clearance of 20 µm; viscosity of 500 Pas)

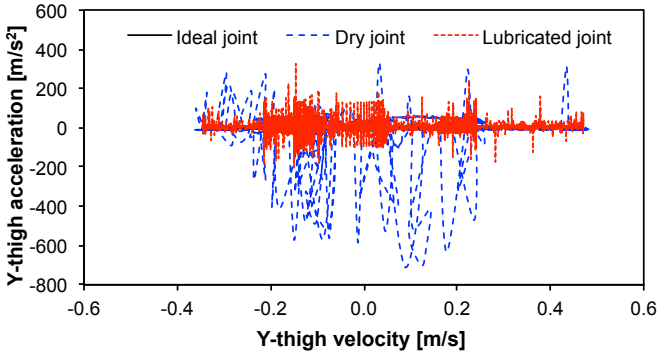

Figure 7: Poincaré map for a complete gait cycle (hip radius of 32 mm, radial clearance of 20 µm; viscosity of 500 Pas)

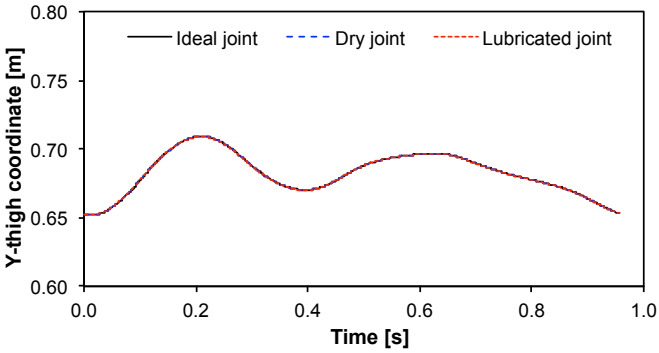

Figure 8: Y-position of the thigh for a complete gait cycle (hip radius of 32 mm, radial clearance of 20 µm; viscosity of 250 Pas)

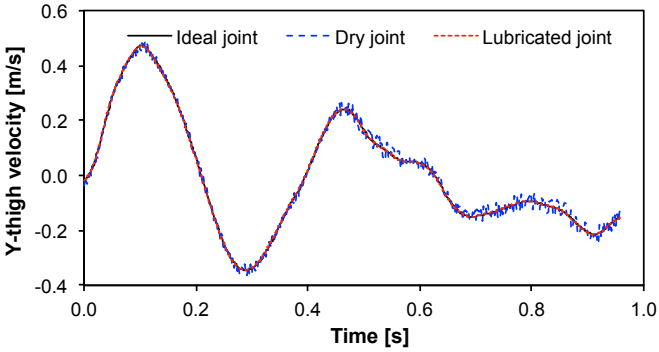

Figure 9: Y-velocity of the thigh for a complete gait cycle (hip radius of 32 mm, radial clearance of 20 µm; viscosity of 250 Pas)

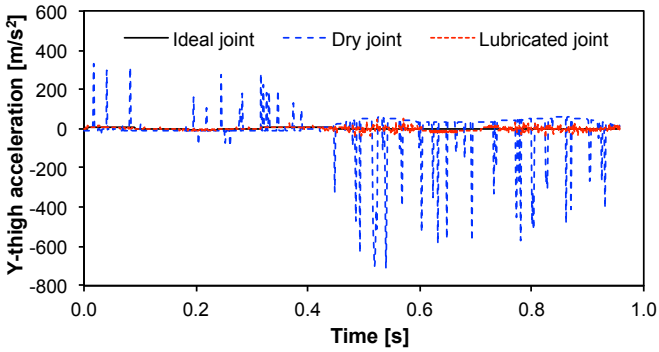

Figure 10: Y-acceleration of the thigh for a complete gait cycle (hip radius of 32 mm, radial clearance of 20 µm; viscosity of 250 Pas)

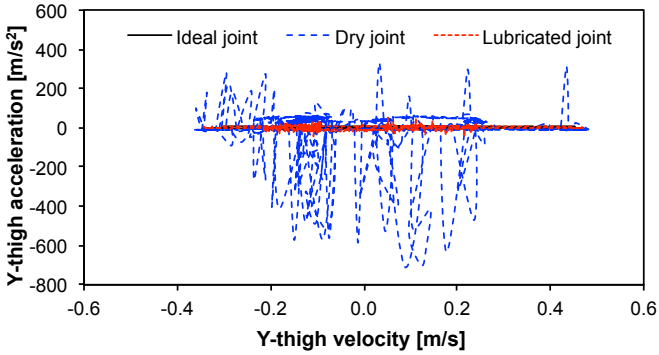

Figure 11: Poincaré map for a complete gait cycle (hip radius of 32 mm, radial clearance of 20 µm; viscosity of 250 Pas)

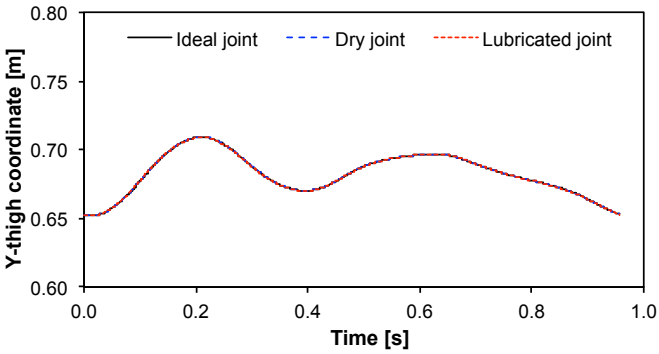

Figure 12: Y-position of the thigh for a complete gait cycle (hip radius of 28 mm, radial clearance of 20 µm; viscosity of 250 Pas)

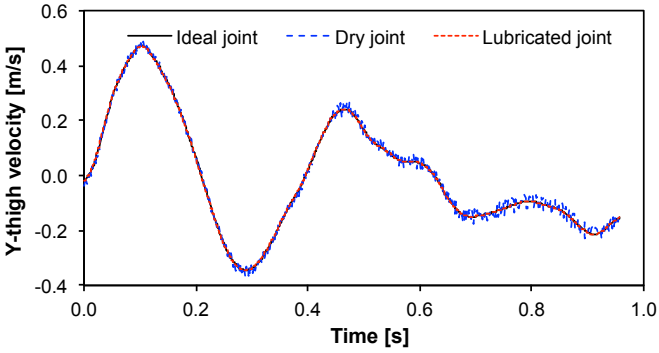

Figure 13: Y-velocity of the thigh for a complete gait cycle (hip radius of 28 mm, radial clearance of 20 µm; viscosity of 250 Pas)

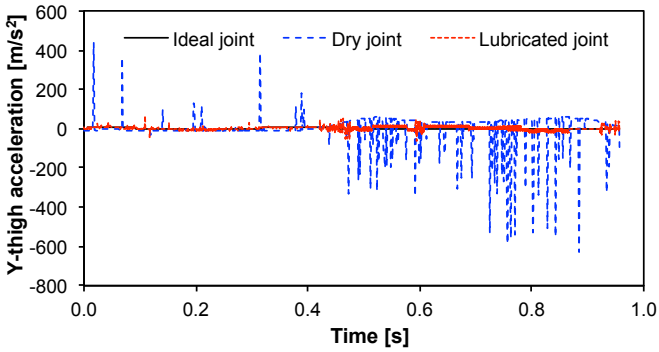

Figure 14: Y-acceleration of the thigh for a complete gait cycle (hip radius of 28 mm, radial clearance of 20 µm; viscosity of 250 Pas)

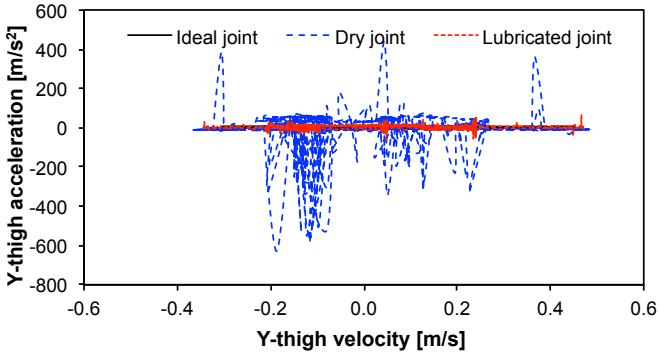

Figure 15: Poincaré map for a complete gait cycle (hip radius of 28 mm, radial clearance of 20 µm; viscosity of 250 Pas)

7. CONCLUSIONS

In this work, the effect of using different hip joint models on a human multibody model has been investigated. For this purpose, ideal kinematic, dry, and lubricated approaches have been considered to model the human hip articulation. This work has been developed under the framework of planar multibody systems formulation.

The response of the human multibody model has been quantified by the examinations of the main kinematic variables for a complete gait cycle, namely in terms of positions, velocities and accelerations of the thigh. Additionally, Poincaré maps have been constructed to analyze the dynamic behavior of the system. In general, it can be drawn that the system's response tends to be smooth for the lubricated modeling case, in particular when the synovial fluid viscosity is not very high. For the case of dry joint model, it can be observed that the intra-joint contact forces cause high peaks on the acceleration plots and also tend to produce a nonlinear response in terms of Poincaré diagrams.

In short, the methodologies and modeling approaches as well as the results provided in this work show a potential towards the better understanding of the complex mechanical behavior of the human hip articulation. As future developments, the effect of the hip joint model on the muscles activation must be taken into account, and also some experimental investigation is needed to validate the methodologies presented in this work. Another important issue that must be considered is the presence of cartilages and how they can influence the human multibody model responses. Finally, it would also be of great important to extend the present investigation to the three-dimensional case, when the human hip articulation can be modeled as a ball and socket element.

ACKNOWLEDGMENTS

The first and third authors express their gratitude to the Portuguese Foundation for Science and Technology for the PhD grants SFRH/BD/76573/2011 and SFRH/BD/64477/2009, respectively. The authors would like to thank to the Portuguese Foundation for Science and Technology through the project UID/EEA/04436/2013. The authors are also gratefully acknowledge the financial support from QREN (*Quadro de Referência Estratégico Nacional* - National Strategic Reference Framework), for this study "INOVSHOES - *Padronizar para Customizar Calçado Ortopédico*", project n.º 2010/12032.

REFERENCES

[1] Silva, M.P.T., Ambrosio, J.A.C., 2003. Solution of redundant muscle forces in human locomotion with multibody dynamics and optimization tools. Mechanics Based Design of Structures and Machines, 31, 381-411.

[2] Horsman, K., M.D., Koopman, H.F., van der Helm, F.C., Prosé, L.P., Veeger, H.E., 2007. Morphological muscle and joint parameters for musculoskeletal modelling of the lower extremity. Clinical Biomechanics, 22(2), 239-247.

[3] Arnold, E.M., Ward, S.R., Lieber, R.L., Delp, S.L., 2010. A model of the lower limb for analysis of human movement. Annals of Biomedical Engineering, 38(2), 269-279.

[4] Pereira, A.F., Silva, M.T., Martins, J.M., De Carvalho, M., 2001. Implementation of an efficient muscle fatigue model in the framework of multibody systems dynamics for analysis of human movements. Proceedings of the Institution of Mechanical Engineers, Part K: Journal of Multi-body Dynamics, 225(4), 359-370.
[5] Frey-Law, L.A., Looft, J.M., Heitsman, J., 2012. A three-compartment muscle fatigue model accurately predicts joint-specific maximum endurance times for sustained isometric tasks. Journal of Biomechanics, 45(10), 1803-1808.
[6] Lobo-Prat, J., Font-Llagunes, J.M., Gómez-Pérez, C., Medina-Casanovas, J., Angulo-Barroso, R.M., 2014. New biomechanical model for clinical evaluation of the upper extremity motion in subjects with neurological disorders: An application case. Computer Methods in Biomechanics and Biomedical Engineering, 17(10), 1144-1156.
[7] Castro, A.P.G., Completo, A., Simões, J.A., Flores, P., 2015. Biomechanical behaviour of cancellous bone on patellofemoral arthroplasty with Journey prosthesis: a finite element study. Computer Methods in Biomechanics and Biomedical Engineering, 18(10),1090-1098.
[8] Machado, M., Flores, P., Claro, J.C.P., Ambrósio, J., Silva, M., Completo, A., Lankarani, H.M., 2010. Development of a planar multi-body model of the human knee joint. Nonlinear Dynamics, 60, 459-478.
[9] Wang, W., Jin, Z., Hu, Y., Wang, F., Dowson, D., 2010. Numerical Lubrication Simulation of Metal-on-Metal Hip Joints: Ball-in-Socket Model and Ball-on-Plane Model. Advanced Tribology, 180-181.
[10] Mattei, L., Di Puccio, F., Piccigallo, B., Ciulli, E., 2011. Lubrication and wear modelling of artificial hip joints: A review. Tribology International, 22, 532-549.
[11] Di Puccio, F., Mattei, L., 2015. Biotribology of artificial hip joints, World Journal of Orthopaedics, 6(1), 77-94.
[12] Di Puccio, F., Mattei, L., 2015. A novel approach to the estimation and application of the wear coefficient of metal-on-metal hip implants. Tribology International, 83, 69-76.
[13] Piazza, S.J., Delp, S.L., 2001. Three-dimensional dynamic simulation of total knee replacement motion during a step-up task. Journal of Biomechanical Engineering, 123, 599-606.
[14] Flores, P., Leine, R., Glocker, C., 2012. Application of the nonsmooth dynamics approach to model and analysis of the contact-impact events in cam-follower systems. Nonlinear Dynamics, 69(4), 2117-2133.
[15] Guess, T.M., 2012. Forward dynamics simulation using a natural knee with menisci in the multibody framework. Multibody System Dynamics, 28(1-2), 37-53.
[16] Quental, C., Folgado, J., Ambrósio, J., Monteiro, J., 2012. A multibody biomechanical model of the upper limb including the shoulder girdle. Multibody System Dynamics, 28(1-2), 83-108.
[17] Dumas, R., Moissenet, F., Gasparutto, X., Cheze, L., 2012. Influence of joint models on lower-limb musculo-tendon forces and three-dimensional joint reaction forces during gait. Journal of Engineering in Medicine, 226(2), 146-160.
[18] Ribeiro, A., Rasmussen, J., Flores, P., Silva, L.F., 2012. Modeling of the condyle elements within a biomechanical knee model. Multibody System Dynamics, 28, 181-197.
[19] Flores, P., Lankarani, H.M., 2012. Dynamic response of multibody systems with multiple clearance joints. ASME Journal of Computational and Nonlinear Dynamics, 7(3), 031003 (13p).
[20] Koshy, C.S., Flores, P., Lankarani, H.M., 2013. Study of the effect of contact force model on the dynamic response of mechanical systems with dry clearance joints: computational and experimental approaches. Nonlinear Dynamics, 73(1-2), 325-338.
[21] Tian, Q., Sun, Y., Liu, C., Hu, H., Flores, P., 2013. Elastohydrodynamic lubricated cylindrical joints for rigid-flexible multibody dynamics. Computers and Structures, 114-115,106-120.
[22] Zhang, Z., Xu, L., Flores, P., Lankarani, H.M., 2014. A Kriging Model for the Dynamics of Mechanical Systems with Revolute Joint Clearances. ASME Journal of Computational and Nonlinear Dynamics, 9(3), 031013 (13p).
[23] Askari, E., Flores, P., Dabirrahmani, D., Appleyard, R., 2014. Study of the friction-induced vibration and contact mechanics of artificial hip joints. Tribology International, 70, 1-10.
[24] Erkaya, S., 2103. Trajectory optimization of a walking mechanism having revolute joints with clearance using ANFIS approach. Nonlinear Dynamics, 71(1-2), 75-91.
[25] Gummer, A., Sauer, B., 2012. Influence of Contact Geometry on Local Friction Energy and Stiffness of Revolute Joints. Journal of Tribology, 134(2), 021402-021402-9.
[26] Sun, D., Chen, G., Wang, T., Sun, R., 2014. Wear Prediction of a Mechanism With Joint Clearance Involving Aleatory and Epistemic Uncertainty. Journal of Tribology, 136(4), 041101-041101-8.
[27] Wang, G., Liu, H., Deng, P., 2015. Dynamics Analysis of Spatial Multibody System With Spherical Joint Wear. Journal of Tribology, 137(2), 021605-021605-10.
[28] Fialho, J.C., Fernandes, P.R., Eça, L., Folgado, J., 2007. Computational hip joint simulator for wear and heat generation, Journal of Biomechanics, 40, 2358-2366.
[29] Machado, M., Flores, P., Ambrósio, J., Completo, A., 2011. Influence of the contact model on the dynamic response of the human knee joint. Proceedings of the Institution of Mechanical Engineers, Part-K Journal of Multi-body Dynamics, 225(4), 344-358.
[30] Meireles, F., Machado, M., Silva, M., Flores, P., 2009. Dynamic modeling and analysis of human locomotion using multibody system methodologies. International Journal of Computational Vision and Biomechanics, 2(2), 199-206.
[31] Mattei, L., Di Puccio, F., 2013. Wear Simulation of Metal-on-Metal Hip Replacements With Frictional Contact. Journal of Tribology, 135(2), 021402-021402-11.
[32] Mattei, L., Di Puccio, F., Ciulli, E., 2013. A comparative study of wear laws for soft-on-hard hip implants using a mathematical wear model. Tribology International, 63, 66-77.
[33] Askari, E., Flores, P., Dabirrahmani, D., Appleyard, R., 2014. Nonlinear vibration and dynamics of ceramic on ceramic artificial hip joints: A spatial multibody modelling. Nonlinear Dynamics, 76(2), 1365-1377.
[34] Ouenzerfi, G., Massi, F., Renault, E., Berthier, Y., 2015. Squeaking friction phenomena in ceramic hip endoprosthesis: Modeling and experimental validation. Mechanical Systemsand Signal Processing, 58-59, 87-100.
[35] Askari, E., Flores, P., Dabirrahmani, D., Appleyard, R., 2015. A Computational Analysis of Squeaking Hip Prostheses. Journal of Computational and Nonlinear Dynamics, 10(2), 024502-7.
[36] Nikravesh, P.E., 1988. Computer Aided Analysis of Mechanical Systems. Prentice Hall, Englewood Cliffs, New Jersey.
[37] Machado, M., Costa, J., Seabra, P., Flores, P., 2012. The effect of the lubricated revolute joint parameters and hydrodynamic force models on the dynamic response of planar multibody systems. Nonlinear Dynamics, 69(1-2), 635-654.
[38] Lopes, D.S., Silva, M.T., Ambrósio, J.A., Flores, P., 2010. A mathematical framework for contact detection between quadric and superquadric surfaces. Multibody System Dynamics, 24(3), 255-280.
[39] Ahmed, S., Lankarani, H.M., Pereira, M.F.O.S., 1999. Frictional Impact Analysis in Open Loop Multibody Mechanical System. Journal of Mechanical Design, 121, 119-127.
[40] Flores, P., Ambrósio, J., 2010. On the contact detection for contact-impact analysis in multibody systems. Multibody System Dynamics, 24(1), 103-122.
[41] Machado, M., Moreira, P., Flores, P., Lankarani, H.M., 2012. Compliant contact force models in multibody dynamics: evolution of the Hertz contact theory. Mechanism and Machine Theory, 53, 99-121.
[42] Hunt, K.H., Crossley, F.R.E., 1975. Coefficient of restitution interpreted as damping in vibroimpact. Journal of Applied Mechanics, 7, 440-445.
[43] Lankarani, H.M., Nikravesh, P.E., 1990. A contact force model with hysteresis damping for impact analysis of multibody systems. Journal of Mechanical Design, 112, 369-376.

[44] Alves, J., Peixinho, N., Silva, M.T., Flores, P., Lankarani, H., 2015. A comparative study on the viscoelastic constitutive laws for frictionless contact interfaces in multibody dynamics. Mechanism and Machine Theory, 85, 172-188.
[45] Lankarani, H.M., Pereira, M.F.O.S., 2001. Treatment of impact with friction in planar multibody mechanical systems. Multibody System Dynamics, 6(3), 203-227.
[46] Herbert, R.G., McWhannell, D.C., 1977. Shape and frequency composition of pulses from an impact pair. Journal of Engineering for Industry, 99, 513-518.
[47] Lee, T.W., Wang, A.C., 1983. On the dynamics of intermittent-motion mechanisms, Part 1: Dynamic model and response. Journal of Mechanisms, Transmissions, and Automation in Design, 105, 534-540.
[48] Gonthier, Y., McPhee, J., Lange, C., Piedboeuf, J-C., 2004. A regularized contact model with asymmetric damping and dwell-time dependent friction, Multibody System Dynamics, 11, 209-233.
[49] Flores, P., Machado, M., Silva, M.T., Martins, J.M., 2011. On the continuous contact force models for soft materials in multibody dynamics. Multibody System Dynamics, 25, 357-375.
[50] Khulief, Y.A., 2013. Modeling of impact in multibody systems: An overview. Journal of Computational and Nonlinear Dynamics, 8, 0210121-15.
[51] Goldsmith, W., 1960. Impact - The theory and physical behaviour of colliding solids. Edward Arnold Ltd, London, England.
[52] Pinkus, O., Sternlicht, S.A., 1961. Theory of Hydrodynamic Lubrication. McGraw Hill, New York.
[53] Nikravesh, P.E., 2007. Initial condition correction in multibody dynamics. Multibody System Dynamics, 18, 107-115.
[54] Baumgarte, J., 1972. Stabilization of Constraints and Integrals of Motion in Dynamical Systems. Computer Methods in Applied Mechanics and Engineering, 1, 1-16.
[55] Flores, P., Machado, M., Seabra, E., Silva, M.T., 2011. A parametric study on the Baumgarte stabilization method for forward dynamics of constrained multibody systems. ASME Journal of Computational and Nonlinear Dynamics, 6(1), 011019 (9p).
[56] Gear, W.W., 1971. Numerical Initial Value Problems in Ordinary Differential Equations. Prentice-Hall, Englewood Cliffs, New Jersey.
[57] Shampine, L., Gordon, M., 1975. Computer Solution of Ordinary Differential Equations: The Initial Value Problem. Freeman, San Francisco.
[58] Winter, D.A., 2005. Biomechanics and Motor Control of Human Movement, 3rd Ed., John Wiley & Sons, Inc, New York.
[59] Meireles, F., 2007. Kinematics and dynamics of biomechanical models using multibody systems methodologies: A computational and experimental study of human gait, MSc Dissertation, University of Minho, Guimarães, Portugal.
[60] Silva, M., Ambrosio, J., 2004. Sensitivity of the results produced by the inverse dynamics analysis of a human stride to perturbed input data. Gait and Posture, 19, 35-49.
[61] Ros, J., Font-Llagunes, J.M., Plaza, A., Kövecses, J., 2015. Dynamic considerations of heel-strike impact in human gait. Multibody System Dynamics, 35(3), 215-232
[62] Gholami, F., Pàmies-Vilà, R., Kövecses, J., Font-Llagunes, J.M., 2015. Effects of foot modelling on the human ankle kinematics and dynamics. Mechanism and Machine Theory, 93, 175-184
[63] Mabuchi, K., Sakai, R., Ota, M., Ujihira, M., 2004. Appropriate radial clearance of ceramic-on-ceramic total hip prostheses to realize squeeze-film lubrication. Clinical Biomechanics, 19(4), 362-9.

LIST OF FIGURE CAPTIONS

Figure 1: Journal-bearing in a planar multibody system representing the hip joint in this study

Figure 2: Two-dimensional human multibody model

Figure 3: The shank-foot subpart of the human multibody model

Figure 4: Y-position of the thigh for a complete gait cycle (hip radius of 32 mm, radial clearance of 20 μm; viscosity of 500 Pas)

Figure 5: Y-velocity of the thigh for a complete gait cycle (hip radius of 32 mm, radial clearance of 20 μm; viscosity of 500 Pas)

Figure 6: Y-acceleration of the thigh for a complete gait cycle (hip radius of 32 mm, radial clearance of 20 μm; viscosity of 500 Pas)

Figure 7: Poincaré map for a complete gait cycle (hip radius of 32 mm, radial clearance of 20 μm; viscosity of 500 Pas)

Figure 8: Y-position of the thigh for a complete gait cycle (hip radius of 32 mm, radial clearance of 20 μm; viscosity of 250 Pas)

Figure 9: Y-velocity of the thigh for a complete gait cycle (hip radius of 32 mm, radial clearance of 20 μm; viscosity of 250 Pas)

Figure 10: Y-acceleration of the thigh for a complete gait cycle (hip radius of 32 mm, radial clearance of 20 μm; viscosity of 250 Pas)

Figure 11: Poincaré map for a complete gait cycle (hip radius of 32 mm, radial clearance of 20 μm; viscosity of 250 Pas)

Figure 12: Y-position of the thigh for a complete gait cycle (hip radius of 28 mm, radial clearance of 20 μm; viscosity of 250 Pas)

Figure 13: Y-velocity of the thigh for a complete gait cycle (hip radius of 28 mm, radial clearance of 20 μm; viscosity of 250 Pas)

Figure 14: Y-acceleration of the thigh for a complete gait cycle (hip radius of 28 mm, radial clearance of 20 μm; viscosity of 250 Pas)

Figure 15: Poincaré map for a complete gait cycle (hip radius of 28 mm, radial clearance of 20 μm; viscosity of 250 Pas)

LIST OF TABLE CAPTIONS

Table 1: Anthropometric data for each anatomical segment of the human multibody model

Table 2: Parameters used in the dynamic simulations of the human multibody model with nonideal hip joint